Research Article
Araştırma Makalesi

Bartın University International Journal of Natural and Applied Sciences
JONAS, 6(2): 189-205 e-ISSN: 2667-5048
31 Aralık/December, 2023 DOI: 10.55930/jonas.1374658

ADSORPTION OF DEEP RED ON AC PREPARED FROM CHESTNUT SHELL

Uğur Selengil[1], Derya Yıldız[1], Burcu Tan[2*]
[1] Eskişehir Osmangazi University, Faculty of Engineering and Architecture, Department of Chemical Engineering, 26040, ESKİŞEHİR
[2] Çanakkale Onsekiz Mart University, School of Graduate Studies, 17020, ÇANAKKALE

Abstract

Adsorption of Deep Red (DR) on activated carbon (AC) produced from chestnut shell has been studied. Chemical activation process with ZnCl2 was applied to the ground chestnut shells at 3:1 ($ZnCl_2$/Raw Material) impregnation ratio, and then at 500 °C, the carbonization process was used to produce AC. The surface area of the AC was defined as 2187 m^2/g. Effects of AC dose, contact time, pH, temperature and initial concentration on DR adsorption have been studied. In experimental studies, 97.4% dye removal was achieved using 0.1 g AC at pH 2.5, 45°C and at 100 mg/L. Dye removal has been seen to increase at all initial concentrations as the temperature increased. The kinetic data are corresponding to the pseudo 2nd order kinetic model. The finding was that the adsorption process corresponding to the Freundlich isotherm model. According to ΔS, ΔH, and ΔG thermodynamic data, DR adsorption on AC is an endothermic and chemical adsorption. The study's findings revealed that AC prepared from chestnut shell is suitable for removing DR from aqueous solutions.

Key Words: Adsorption, Deep Red, Activated Carbon, Chestnut Shell

1. Introduction

Water is essential to life, but the freshwater resources on earth are decreasing every year. The low amount of precipitation as an effect of climate change, uncontrolled agricultural irrigation and excessive water consumption are the biggest reasons for this (Dutta et al., 2021). Pollution of these diminishing resources for various reasons also endanger usable water resources. Discharge of industrial wastes to fresh water resources is one of the main pollution factors. The textile industry consists of processes that use a lot of water and produce excess wastewater. Dyes constitute a large part of the pollution in textile wastewater. Many dyestuffs such as basic, acidic, reactive and pigment are used in the textile industry. It is known that about 60% of the initial amount of such dyes, especially for cotton fabrics, passes into wastewater (Rivera et al., 2011). Azo dyes have one or more -N=N- on the aromatic rings. Deep Red (DR) is in the class of azo dyes (CAS:3564-22-5). The structure of the DR is given in Figure 1. The IUPAC name, molecular formula and molecular weight is (4Z)-4-[(4-methyll-2-nitrophenyl) hydrozinlidin]-N-(3-nitrophenyl)-3-oxynaphthalene-2-carboxyamide, $C_{24}H_{17}N_5O_6$, 471.42 g/mol, respectively.

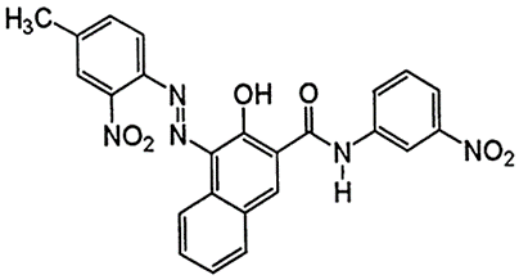

Fig. 1 DR (Pigment Red 18)

The removal of dyes, which cause serious health and ecological problems, from wastewater is gaining importance day by day. Many methods such as advanced oxidation techniques, electrolysis, filtration, ion exchange coagulation and adsorption have been applied for the dye removal (Bal & Thakur, 2022; Aragaw & Bogale, 2021).

***Corresponding Author:**
Burcu TAN Çanakkale Onsekiz Mart University, School of Graduate Studies
17020, Çanakkale-Turkey.

Geliş (Received) : 11.10.2023
Kabul (Accepted) : 07.11.2023
Basım (Published) : 31.12.2023

In terms of ease of use and cost, adsorption is the most advantageous of these methods. Adsorption has been studied by many researchers as a highly efficient, sustainable and environmentally friendly method for the dye removal from wastewater.

Natural clay (Al Kausor et al., 2022; Bergaoui et al., 2018), MOFs (Beydaghdari et al., 2022), polymeric adsorbents (Li et al., 2022; Saini & Dey, 2022), magnetic nanoparticles (Bayantong et al., 2021) and ACs (Sh. Gohr et al., 2022; Xue et al., 2023) were used to increase the dye adsorption yield. Various adsorbents used for the azo group dye adsorption and their adsorption capacities are given in Table 1.

Table 1. Various adsorbents used for adsorbing some azo dyes and their adsorbing capacities

Dye	Adsorbent	q (mg/g)	References
Basic Red 18	Nano-clay	714.3	Hasani et al. (2017)
Basic Red 18	Perfil	12.82	Maximova& Koumanova (2008)
Basic Red 18	Hydrochared waste human hair	84.95	Isik et al. (2022)
Basic Red 46	Moroccan clay	54	Bennani Karim et al. (2009)
Acid Red 18	Magnetic porous polymer composite	301	Lu et al. (2019)
Acid Red 18	Peach stone AC	34.32	Saratele et al. (2016)
Acid Red 18	Zeolite/Chitosan Hydrogel	332.48	Hidayat et al. (2022)
Congo red	Fe_3O_4@Al-MOF	2446.18	Kang et al. (2023)
Congo red	Zinc curcumin oxide nanoparticles	94.45	Arab et al. (2022)
Congo red	Carbon stem of water hyacinth	14.367	Extross et al. (2023)
Congo-red	Ca-bentonite	107.41	Lian et al. (2009)
Reactive red 120	Fouchana clay	9.3	Errais et al. (2012)
Deep red	Organo bentonite modified with cetyltrimethylammonium bromide	38.81	Tumsek (2019)
DR (Pigmet Red 18)	Chestnut AC	45.85	This study

Among the adsorbents used for removal of dye, the ACs obtained from biomass are cheap and sustainable. High adsorption capacity is also an important advantage for dye removal. AC can be made from many different materials. Selected materials should be cheap and abundant for economy and efficiency (Husien et al., 2022). In particular, waste biomass resources have a high potential in this respect. ACs, which have advanced surface properties, can be made by physical and chemical process. Adsorption capacities of ACs are determined by surface properties. The activation agent's chemical composition, in particular, has an impact on the AC's functional groups. It is stated that these surface groups are in charge of the the adsorption process (Husien et al., 2022). Thanks to these properties, AC is a very suitable adsorbent for waste water (Aragaw & Bogale, 2021). ACs produced from many different biomass sources are frequently used for dye removal from waste water. For example, Jawad et al. produced AC from the dragon fruit peel and used it for Methylene Blue (MB) adsorption and the highest capacity was found as 195.2 mg/g in this study (Jawad et al., 2021). Foroutan et al., produce the AC from lemon tree and use it for crystal violet dye adsorption. The most effective parameter was found to be pH and the highest capacity was 23.6 mg/g (Foroutan et al., 2021). AC produced from waste coffee was used in adsorption of Congo Red dye and the max capacity for adsorption was found as 90.9 mg/g (Lafi et al., 2019). In another study, the AC made from Indian Slug Seeds was examined for the Victoria Blue adsorption and the capacity is 92.78 mg/g.

Thermodynamic data have shown that adsorption occurs endothermic and spontaneously (Khan et al., 2022). AC made from cactus fruit peels was used in the Basic Red 46 adsorption and the capacity was obtained as 806.38 mg/g under optimum conditions (Akkari et al., 2023). Chestnut shells have also been a very preferred waste biomass source for AC production. Altintig et al. derived AC from chestnut shells and then deposited magnetic Fe_3O_4 particles. This magnetic AC was used for the Malahite Green (MG) adsorption. It has 311.40 mg/g adsorption capacity in optimum experimental conditions (Altintig et al., 2018). Zhang et al., produced the AC from chestnut shells and used for removal of MB and the 1489.88 mg/g of capacity was found. The surface area of this AC is 1539.41 m^2/g (Zhang et al., 2021). Kong & Zhang (2022), derived an AC with $ZnCl_2$ activation from chestnut shell and applied in methylene blue adsorption. The SBET of the carbon is 1539.4 m^2/g. It has determined that the adsorption process contains chemical adsorption. Capacity for adsorption was found as 1435.87 mg/g (Kong & Zhang, 2022). ACs produced from chestnut shells are used in the adsorption of various heavy metals as well as dye removal. Demiral et al., in their study, produced an AC by H_3PO_4 activation from chestnut shells. A pore volume of 0.7819 cm^3/g and a surface area of 1611 m^2/g have been determined. This AC was used for the lead adsorption (Demiral et al., 2014). Akbari and Olfati used ACs derived from chestnut shell, walnut shell, coconut shell and peanut shells for arsenic adsorption (Akbari & Olfati, 2020). Özçimen & Meriçboyu used ACs made from chestnut shell and grape seeds as adsorban to adsorption the Cu (II) ions. Chestnut shell AC surface area has been found as 1319 m^2/g (Özçimen & Meriçboyu, 2009).

In our study, the adsorption capability of the AC for removing DR dye was investigated after it had been produced by activating $ZnCl_2$ from chestnut shell. A study on DR adsorption with AC produced from chestnut shell by $ZnCl_2$ activation was not performed, although various dye and heavy metal adsorption experiments had been performed with ACs obtained from chestnut shell. Our study is unique for adsortion of DR dye in this regard.

2. Materials and Methods

2.1 AC

$ZnCl_2$ (MERCK) was used as dehydration agent in active carbon production from chestnut shell. The selected impregnation ratio was 3:1 ($ZnCl_2$/Chestnut shell). For the impregnation process, 90 g $ZnCl_2$ was dissolved in 300 ml of distilled water. 30 g of ground chestnut shells were added to the $ZnCl_2$ solution and mixed for 6 h at 75 °C in the magnetic mixer. After the impregnation process, the aqueous solution was filtered and the remaining solid part was dried for 24 h at 105 °C. The $ZnCl_2$ impregnated chestnut shell was placed in a stainless steel vessel and carbonized in a vertical furnace (Carbolite TZF 12/75/700). The obtained sample was carbonized at 500 °C. 100 mL/min was the chosen the N_2 flow rate and the heating rate to 10 °C/min. Following carbonization, AC and a 0.5 N HCl acid solution were mixed for one hour. Then it was washed until the pH was between 6-7 with hot distiled water then dried for 24 h. The N_2 gas adsorption-desorption isotherm in 77 K was used to identify the surface characteristics of the AC (Autosorb 1C (Quantachrome)). The functional groups of AC were determined using an FT-IR instrument (The Bruker Tenor 27). Surface morphology of AC was determined by SEM analysis (Hitachi Regulus 8230). Elemental analysis of AC is performed with EDS (Energy Dyspursive Spectroscopy).

2.2 Adsorption

The adsorption of Deep Red (DR) was performed in the shaking water bath (Memmert). The absorbance values of the dye solutions were determined at 519 nm wavelength with UV spectrophotometer (Shimadzu). After preparing a 1000 mg/L stock solution from DR dye, by diluting the stock solution, dye solutions at different concentrations were prepared. On adsorption, the effects of the solution's pH, dye concentration, amount of AC, contact time, and temperature were examined and the most appropriate conditions for dye removal were determined. All experiments performed in 50 ml dye solution. To be able to study the pH effect, the samples were shaken for 24 hours at 25 °C at different pH values ranges between 2.5 to 11.0 at a 100 mg/L concentration. HCl and NaOH were utilized for pH adjustments of dye solutions. To be able to examine the effect of adsorban dose, experiments were conducted for 24 h at pH 2.5, 25 °C and 100 mg/L concentration by using adsorban in the range of 0.025-0.2 g. For the purpose of calculating the equilibrium time, experiments were conducted at 25 °C, 100 mg/L initial concentration, pH 2.5 with 0.1 g of AC. During the adsorption process, samples were taken at regular intervals for 0.5-72 h and concentrations of samples were calculated. With the obtained results, the most suitable kinetic model for the DR adsorption was determined. It was studied at pH 2.5 values to investigate how temperature affects and dye concentration. In research on adsorption, 0.1 g of AC was included in to the dye solutions made with various concentrations in the range of 100-500 mg/L. Adsorption experiments were conducted at 25, 35 and 45 °C for 24 h. At the conclusion of the period of time, the absorbance values of the samples were read at 519 nm wavelength and their concentrations were calculated.

The compatibility of the results obtained with the models of the Freundlich and Langmuir isotherms has been studied. Equation (1) was utilized to determined the quantitiy of dye adsorbed each unit of AC.

$$q_e = \frac{C_0 - C_e}{m} V \quad (1)$$

q_e : Adsorbed DR on unit adsorbent (mg/g)
C_o : Initial DR concentration (mg/L)
C_e : Equilibrium concentration of dye solution (mg/L)
V : Volume of the solution (L)
m : Adsorbant dose (g)

The percentage of dye removed from the solution was determined according to the Equation (2).

$$\text{Removal}\,\% = \frac{C_0 - C_e}{C_0} \quad 100 \quad (2)$$

2.3 Kinetics

Pseudo-1st-order, 2nd-order and intra-particle diffusion models were used to analyze the kinetic data. The Equation (3) derived by Lagergren (Demiral et al., 2008; Sharma & Bhattacharyya, 2005) is used to determine the adsorption rate constant for pseudo-first order.

$$\log(q_e - q) = \log q_e - \frac{k_1}{2.303} t \quad (3)$$

Pseudo 1st order rate constant is k_1 (h^{-1}), the amount of DR that was adsorbed on a unit amount of AC at time t is shown by the symbol q_t (mg/g). The contact time represented by the t (h). The slope of the log (q_e-q_t) plot against t is used for finding the constants k_1 and n. (Figure 10).

Pseudo-2nd-order equation expression according to Equation (4) (Demiral et al., 2008),

$$\frac{t}{q} = \frac{1}{k_2 q_e^2} + \frac{t}{q_e} \quad (4)$$

Pseudo 2nd order rate constant is k_2 (g $mg^{-1}.h^{-1}$), The contact time is indicated by the symbol t (st). When t/q_t and t graphs are drawn, the slope of the line represents $1/q_e$. The intersection point of the line represents $1/(k_2.(q_e)^2)$. (Figure 11).
The intra-particle diffusion is expressed as Equation (5) (Shakoor & Nasar, 2016; Selengil & Yıldız, 2022),

$$q_t = k_i t^{1/2} + C \quad (5)$$

ki ($mg/g.min^{1/2}$) is the intra-particle diffusion rate constant (Figure 12). k_i value is taken from the slope of the line q_t drawn versus $t^{1/2}$ and the line's intercept is used to find out the constant C. Table 2 displays the constants for the kinetic models.

2.4 Isotherms

The fact that the adsorption isotherm is compatible with the Langmuir isotherm model indicates that monolayer adsorption takes place on a homogeneous surface. The fact that the isotherm is compatible with the Freundlich model. According to this model, the multilayer adsorption is likely to take place on a heterogeneous surface (Yorgun et. al., 2017). Equation (6) expresses the Langmuir isotherm model. (Demiral et al., 2008; Yuh-Shan, 2004).

$$\frac{C_e}{q_e} = \frac{1}{Q_0 b} + \frac{C_e}{Q_0} \quad (6)$$

The concentration of DR at equilibrium is C_e (mg/L). The equilibrium adsorption capacity defined as q_e (mg/g) and the adsorption capacity defined as Q_0 (mg/g). b (L/mg) is the adsorption constant. Langmuir adsorption isotherm at 25, 35 and 45 °C is given in Figure 14. The slope and intercept of the plot of C_e/q_e vs C_e were used to calculate the Langmuir constants. R_L, defined in Equation (7), is known as the separation factor (Sharma & Bhattacharyya, 2005; Kavitha & Namasivayam, 2007).

$$R_L = \frac{1}{1 + b\,C_0} \quad (7)$$

The initial concentration of the DR solution is designated C_0 (mg/L). The R_L value takes the value of $0 < R_L < 1$ if the isotherm type is favorable, $R_L > 1$ if unfavorable, $R_L = 1$ if linear or $R_L = 0$ if irreversible (Liu et al., 2012). Equation (8) gives the Freundlich isotherm's definition. (Selengil & Yıldız, 2022).

$$\ln q_e = \ln K_f + \frac{1}{n} \ln C_e \quad (8)$$

where, adsorption capacity is measured by K_f (L/g), while intensity is defined by the isotherm constant n. Figure 15 displays the $\ln(C_e)$ versus $\ln(q_e)$ curves for the adsorption temperatures of 25, 35, and 45 ºC. The slope and intercept of the graph of $\ln q_e$ and $\ln C_e$ were used to determine the values for K_f and n.

2.5 Thermodynamics

Equation (9) and (10) was used to calculate the change in the adsorption's Gibbs energy (ΔG°).

$$K_C = \frac{q_e}{C_e} \quad (9)$$

$$\Delta G° = -RT \ln K_C \quad (10)$$

Where, the temperature is denoted by T (K), and the gas constant by R (8.314 Jmol/K). K_C is the equilibrium constant it is obtained from the Equation (11) (Selengil & Yıldız, 2022). The parameters ΔH° and ΔS° were determined from the slope and intercept of the 1/T vs. ln Kc graph, respectively.

$$\ln K_C = -\frac{\Delta H°}{RT} + \frac{\Delta S°}{R} \quad (11)$$

3. Materials and Methods

3.1 Characterization of AC

The surface characterization of AC produced from chestnut shells was made by N_2 adsorption. N_2 adsorption-desorption isotherms are given in Figure 2. Figure 3 depicts the graph of the distribution of pore sizes.

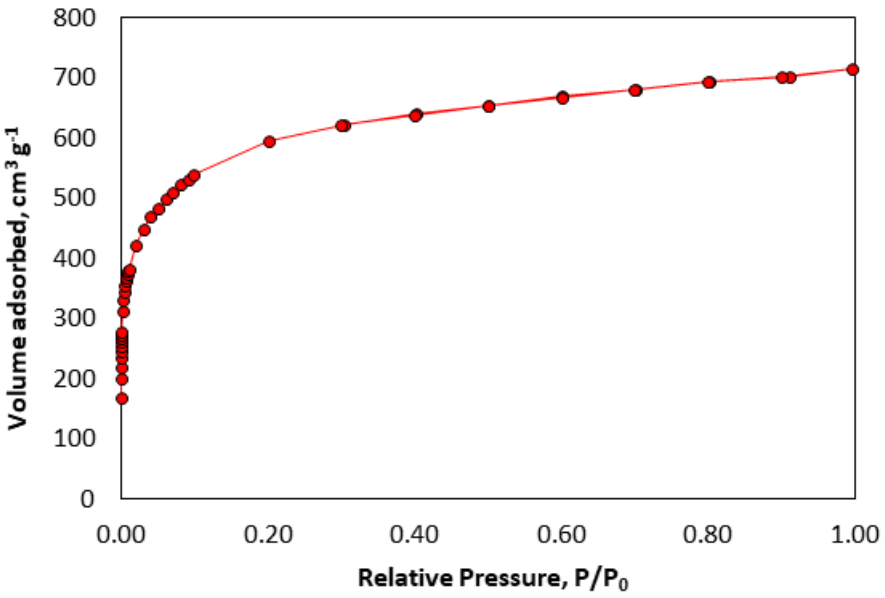

Fig. 2 N_2 isotherm of AC

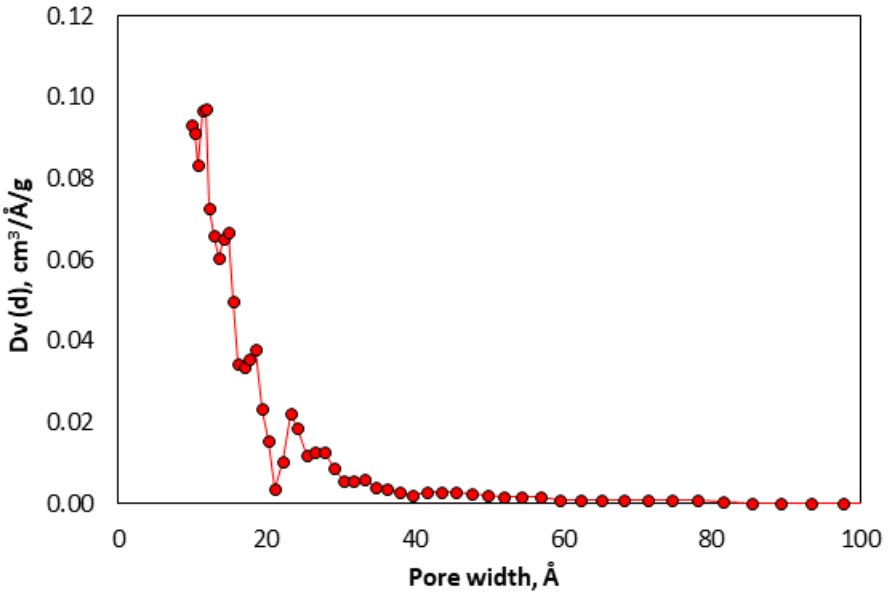

Fig. 3 Pore size distrubution of AC

The AC's N_2 adsorption-desorption isotherm obtained from chestnut shell at 3:1 impregnation ratio and at 500°C is suitable for Type I isotherm. The isotherm rose with a rapid slope up to the point where the relative pressure was 0.1. In this region, the rate of nitrogen adsorption by the pores is high. It is understood that the pores are filled at low relative pressures and this indicates that the AC consists of a microporous structure. In addition, in the isotherm of AC, the adsorption and desorption arms are almost coincident and no hysteresis region is observed. In this case, it can be said that AC contains a high percentage of micropores. At values of relative pressure greater than 0.1, the isotherm proceeded parallel to the horizontal axis and increased upwards until high relative pressures. This situation also shows that AC contains some mesoporous structure.

Figure 3 shows a graph of the distribution of pore sizes. The density of the pores was found to be in the range of 10-30 Å. Observation of significant peaks at values less than 20 Å indicated the presence of micropores. According to pore size distribution figure, it is seen that the highest pore diameter density is around 12 Å. This result indicates that the pore structure of AC is mostly made up of micropores. SBET area and isotherm curves also supported this

result. Calculations revealed that AC has a surface area of 2187 m^2/g, micropore volume 0.770 cm^3/g, total pore volume 1.106 cm^3/g, average pore diameter of 20.23 Å. According to these results, 70% of the total pore volume of AC consists of micropores. It can be said that AC is suitable for adsorption studies because of the presence of the high density of micropores and also presence of the mesopores structure.

The band at approximately 3900-3700 cm^{-1} in the FTIR spectrum of the AC given in Figure 4 is an O-H bond vibration, it demonstrates that there are hydrogen bonds present in water. (Karapınar 2022; Kazemipour et al., 2008; Şencan et al., 2015). The broad band at 3204-3000 cm^{-1} represents stretching vibration of carboxyls, phenols or alcohols or –OH groups (Sun et al., 2016). The band in the 1590-1550 cm^{-1} range explains the C=C aromatic vibration (Shafeeyan et al., 2011; Hesas et al., 2013; Prahas et al., 2008). The band at 1300-1100 cm^{-1} is caused by the C=O vibration found in acids, phenols, alcohols, ethers and/or ester groups (Prahas et al., 2008). It has also been shown that the peaks between 600 and 900 cm^{-1} may originate from C−Cl bonds (Karapınar, 2022).

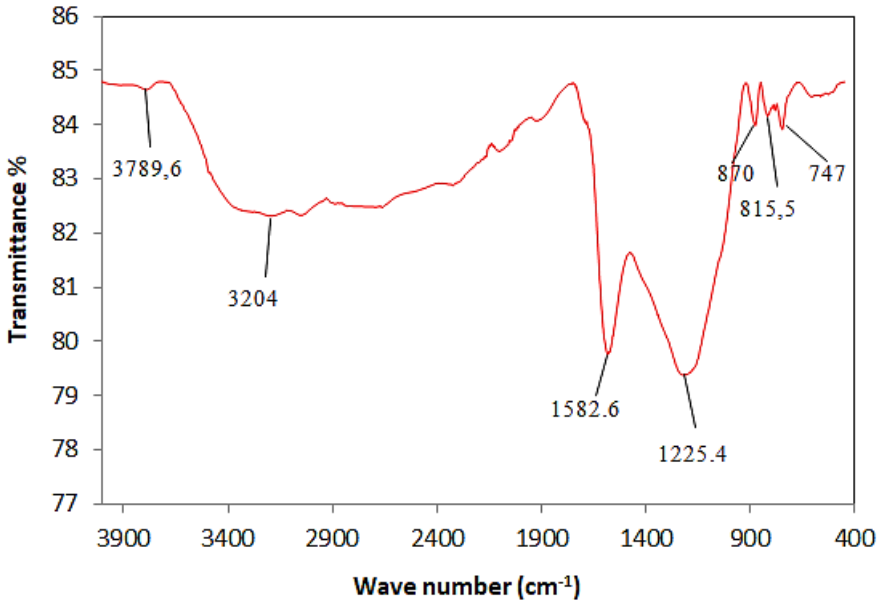

Fig. 4 FTIR spectrum of AC

In order to examine the surface morphology of AC, SEM-EDS analysis was performed, the images are given in Figure 5 and Figure 6.

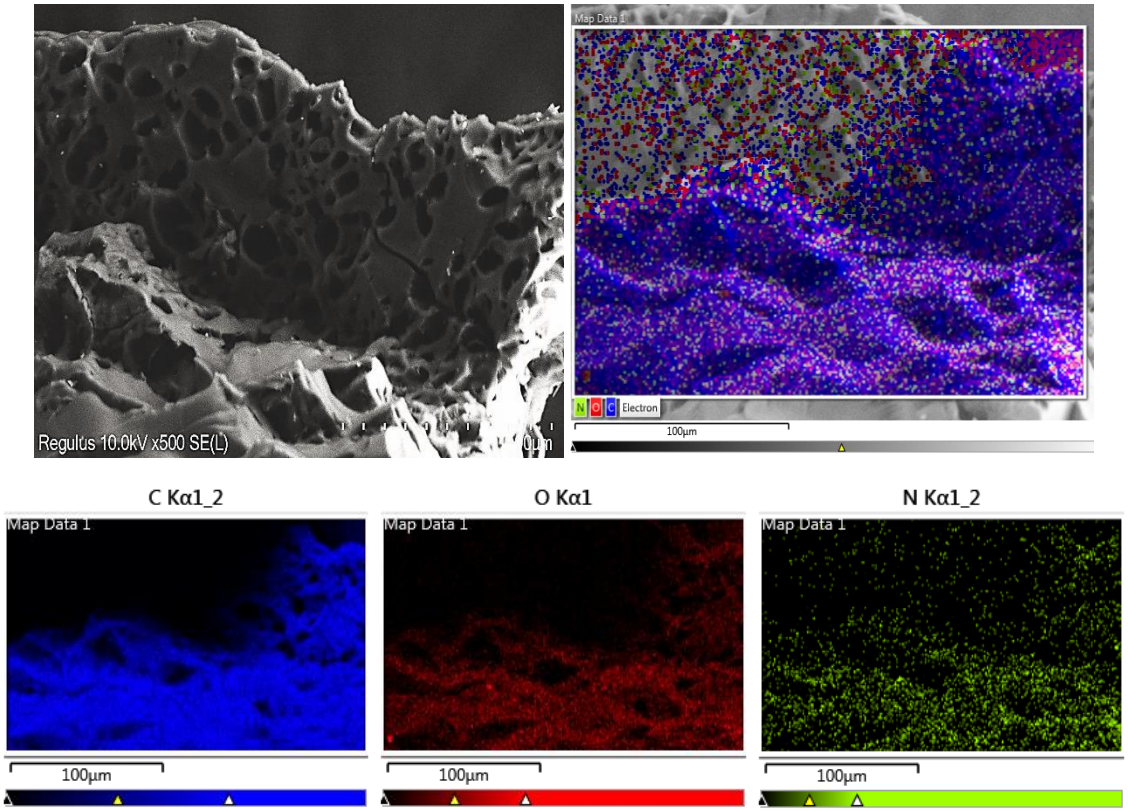

Fig. 5 SEM image and elemental mapping of AC

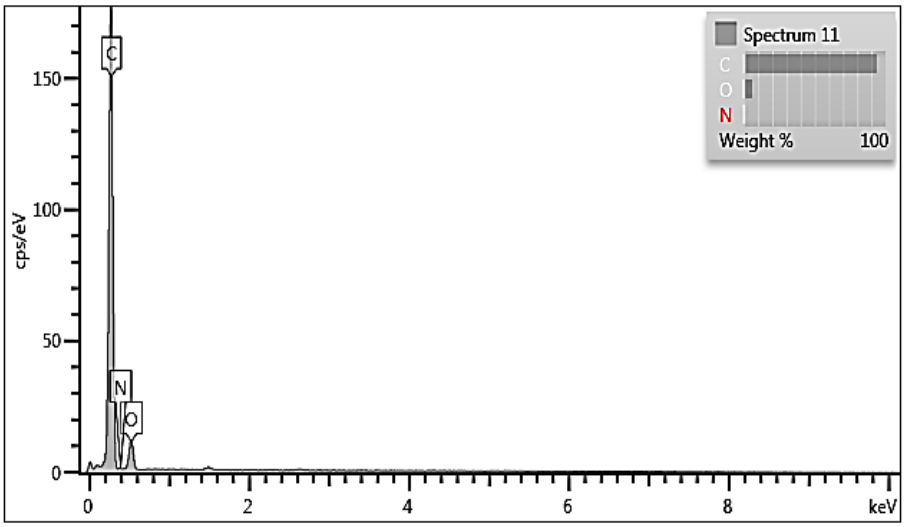

Fig. 6 EDS spectrum of AC

Figure 5 displays the porous structure of AC and the elemental distribution on the surface. In the image taken at 100 µm, there was evidence that the pore structure was continuous inwards and that the pores were not connected to each other at the surface. The pore entrances on the surface are of different sizes and the surface is irregular.

When the EDS result of AC was examined, it was seen that AC contained 93.75% C, 0.47% N, 5.78% O. According to these results, it was determined that AC has high carbon content, micropore structure and a large surface area. Adsorbing capacity of carbon, which has more active sites, is also high, thanks to a large surface area

and micro-porous structure. In this respect, to remove DR from solution by adsorption, AC made from chestnut shells is an appropriate adsorbent.

3.2 Effect of pH

Experiments examining the pH effect on adsorption of DR were performed at 100 mg/L initial concentration of at 25 °C for 24 h. In the experiments, 0.1 g of AC was used and the pH ranges have been changed from 2.5 to 11.0. The results obtained are given in Figure 7.

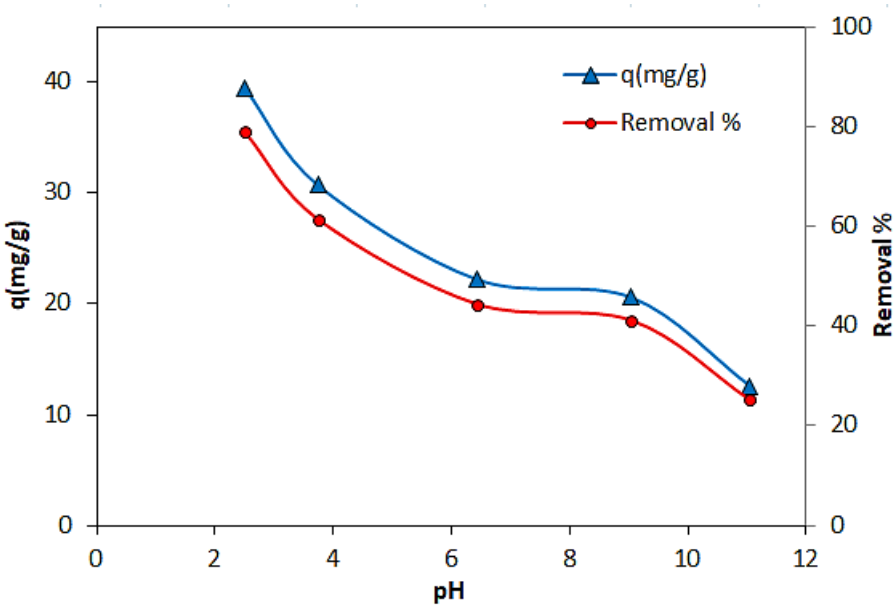

Fig. 7 pH's impact on DR adsorption

At pH 2.5, the highest amount of dye was removed (78.98%) under operating conditions and the q value was found to be 39,49 mg/g. When the results were examined, There was a finding that the dye removal and the q value decreased as the pH increased. At low pH values, positive ions predominate on the adsorbent surface due to H^+ ions, and reactive dyes exist as negatively charged ions in aqueous media. There is an increase in the electrostatic attraction forces because of the opposite charges between the positively charged adsorbent surfaces and the negative dye ions. The increase in capability for adsorption at low pH level is thus explained by electrostatic attraction forces. In the next experimental studies to be carried out with DR, at 2.5 pH adjustment was made to the solution.

3.3 Effect of the adsorbent amount

Experiments were performed to investigate the impact of adsorbent dose at a concentration of 100 mg/L, at pH 2.5 and at 25°C for 24 h. The adsorbent dose was determined between 0.025 and 0.2 g. Obtained results are given in Figure 8.

At the end of 24 hours, 88% DR removal was accomplished by adding of 0.1 g AC. It was calculated that the removal % rised as the adsorbent dose rised. Approximately 96% removal was observed at the end of 24 h with 0.2 g of AC.

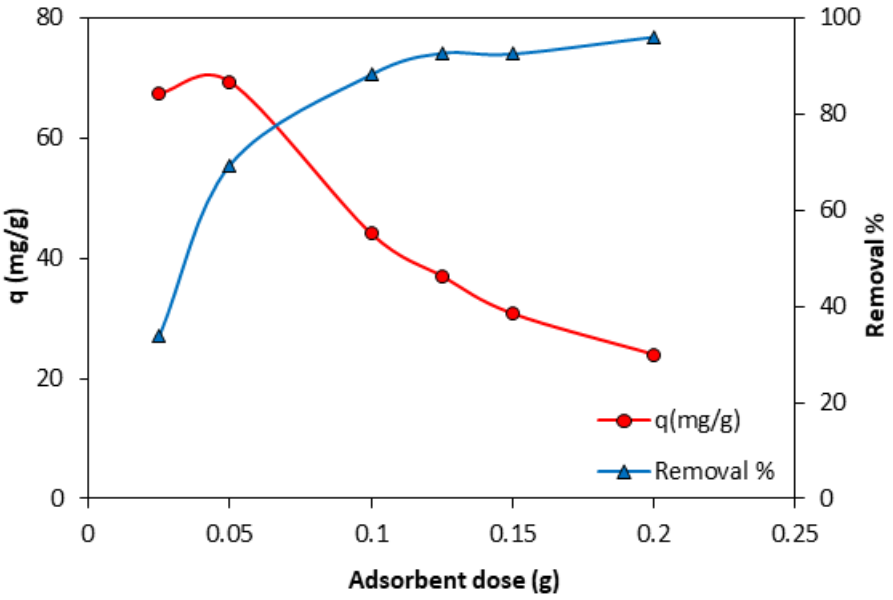

Fig. 8 Adsorbent dose's impact on DR adsorption

3.4 Adsorption Kinetics

To determine the equilibrium time, experiments were conducted at an initial concentration of 100 mg/L including 0.1 g AC at pH 2.5 and 25 °C. Samples were taken at the specified time intervals and the value of absorbance was read in the UV spectrophotometer. Figure 9 depicts the impact of contact time on DR adsorption.

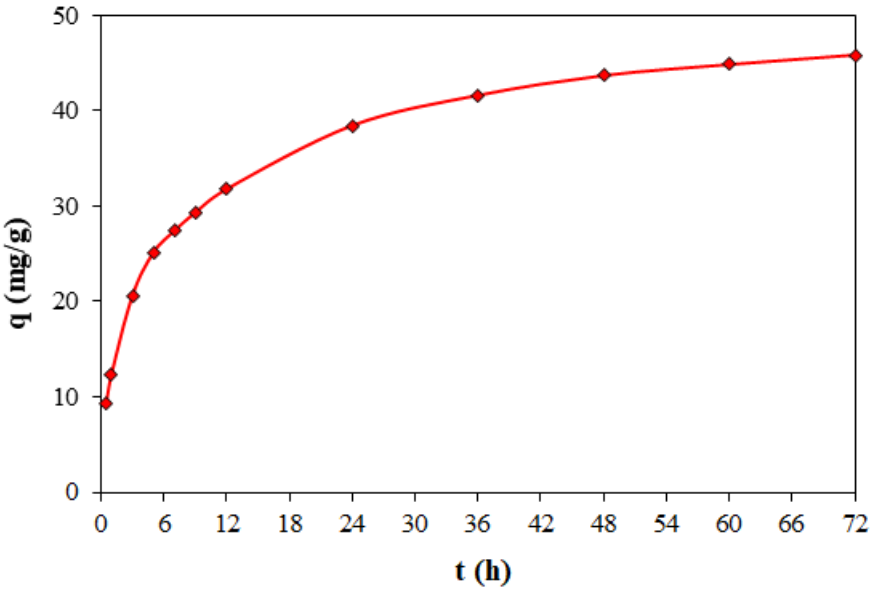

Fig. 9 Effect of contact time on DR adsorption

It is spotted that DR adsorption achieved equilibrium at approximately 72 h, but after 48 h, the removal % (87.4%-91.7%) and the rate of increase of q values (43.7 - 45.9 mg/g) decreased. Consequently, it may be stated that the adsorption achieves equilibrium in 48 h. The pseudo 1st order, pseudo 2nd order and intra-particle diffusion models have been applied. The graphs are given in Figure 10, 11 and 12, respectively, and Table 2 displays the constants of the kinetic model.

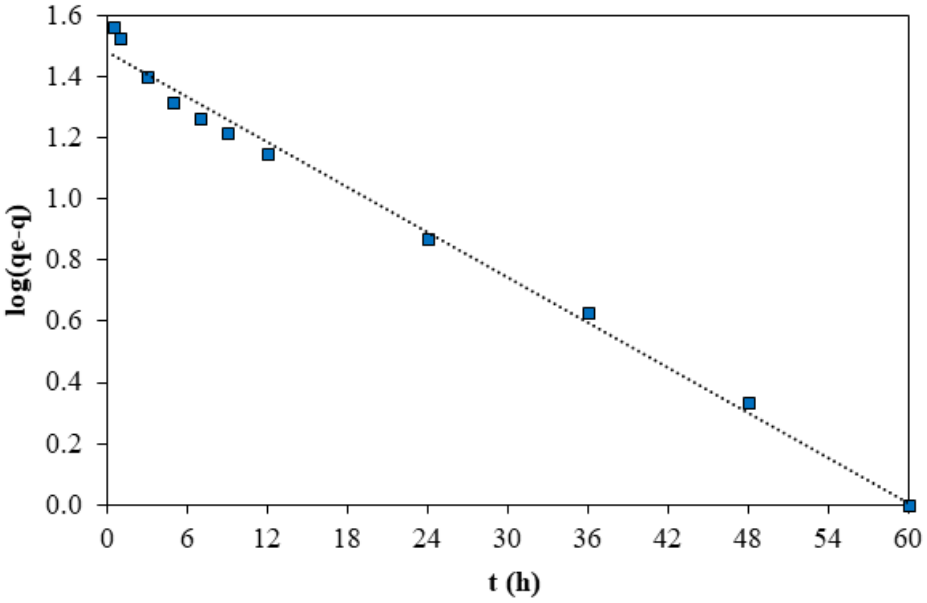

Fig. 10 Adsorption kinetics using a pseudo-first-order model

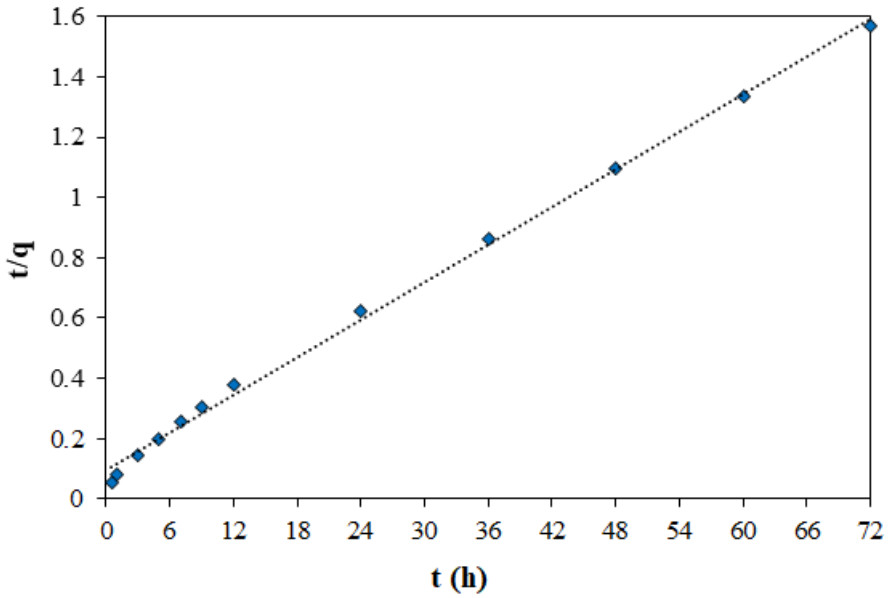

Fig. 11 Adsorption kinetics using a pseudo-second-order model

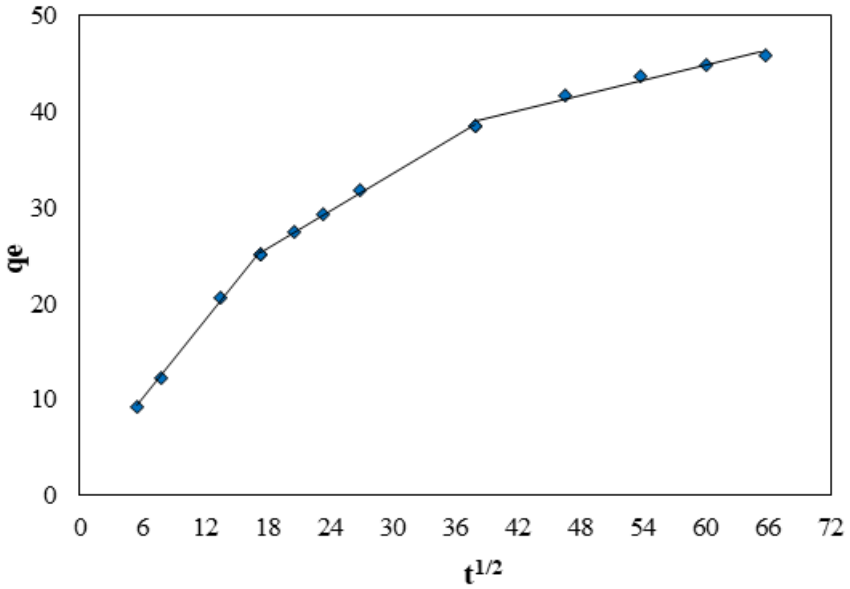

Fig. 12 Intra-particle diffusion model

Table 2. Kinetic constants for pseudo-1st-order, pseudo-2nd-order, and intra-particle diffusion

	pseudo-1st-order			**pseudo-2nd-order**			**intra-particle diffusion**		
q_e (mg/g) (experiment)	k_1 (h^{-1})	q_e (mg/g)	R^2	k_2 (g/mg h)	q_e (mg/g)	R^2	C	k_i (mg/g $min^{1/2}$)	R^2
							1.9018	1.358	0.997
45.849	0.0566	30.451	0.991	0.0046	47.846	0.997	14.245	0.642	0.998
							28.962	0.264	0.972

The pseudo 1st order Lagergren rate constant k1= 0.0566 h^{-1} and the pseudo 2nd order rate constant k2= 0.0046 g $mg^{-1}h^{-1}$. Both kinetic models were revealed to be appropriate for the adsorption of DR on AC. However, according to the correlation coefficients, it is seen that the adsorption kinetics is more appropriate for the pseudo 2nd order model. In addition, the qe values found via experiments and the qe values calculated from the model are very close to each other. In addition, the qe values that found experimentally and the qe that calculated from the model are very close. According to the intra-particle diffusion plot, three phases developed, these phases showed that adsorption proceeds by surface binding and intra-particle diffusion. As the dye concentration in the solution gradually decreased diffusion started to slow down. Examining the diffusion coefficients, we see that the coefficient of the last phase is the lowest. Kinetic results showed that the rate-limiting stage is the chemical adsorption. It has been determined that the DR dyes is attached to the surface of the AC and the adsorption also takes place in the pore by intra-particle diffusion.

3.5 Adsorption Thermodynamics

Experiments were performed at three different temperatures; 25, 35, and 45°C for 24 h to determine the effect of temperature. Experiments conducted at pH 2.5 with 100–500 mg/L initial concentrations and 0.1 g AC. Figure 13 presents the results.

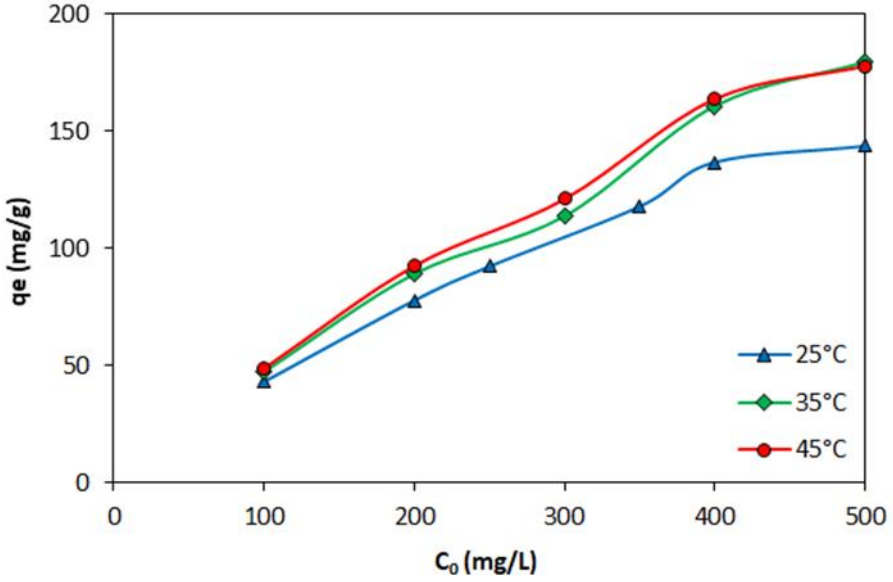

Fig. 13 The effect of temperature and initial concentration

With an increase in the dye's initial concentration, the removal % decreased. Additionally, the quantity of dye absorbed per unit of adsorbent increased. The highest removal percentage was 97.44% in 100 mg/L solution at 45 °C. When the effect of temperature was examined, there was a finding that as the temperature rised, the removal % rised in all initial concentrations. It can be said that as a result of increasing adsorption with increasing temperature, the process proceeds endothermically and chemical adsorption takes place.

Using the obtained data, the suitability of the process to Langmuir and Freundlich models was examined. Calculations of the adsorption of DR according to the Langmuir isotherm model and constants are given in Figure 14 and Table 3. The computation's findings related to the Freundlich isotherm model are shown in Figure 15 and Table 3.

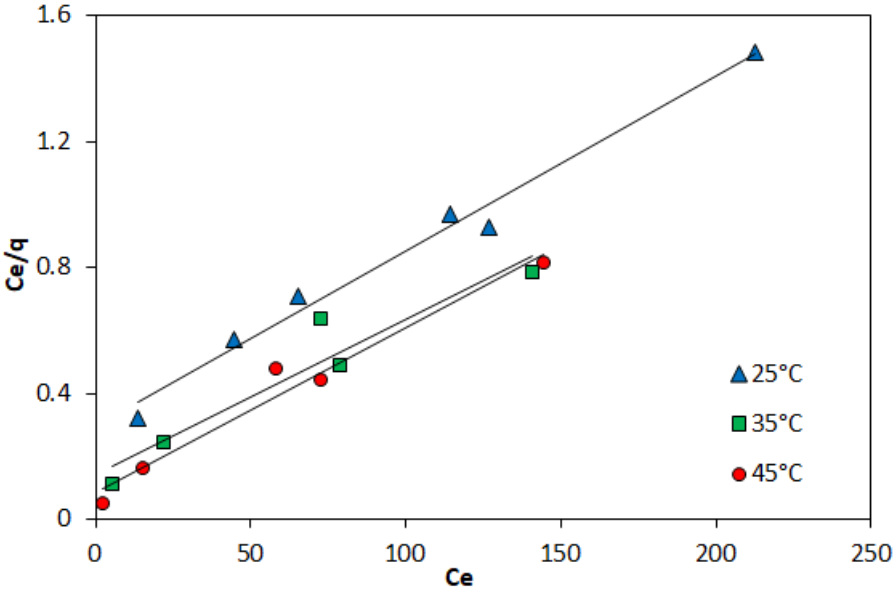

Fig. 14 Isotherms of Langmuir at various temperatures

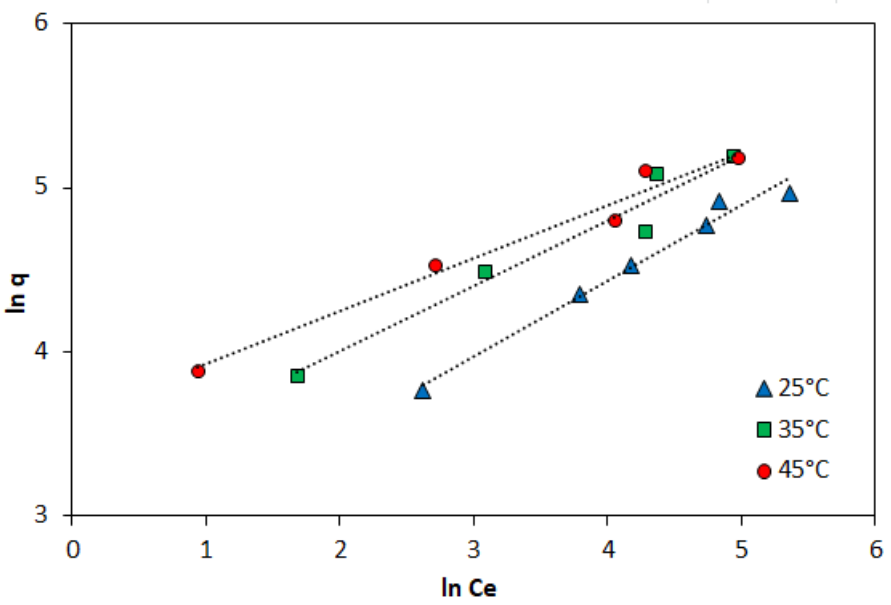

Fig. 15 Isotherms of Freundlich at various temperatures

Table 3. Constants of the Langmuir isotherm for DR adsorption

Temperature (°C)	Langmuir				Freundlich		
	Q_0 (mg/g)	b (L/mg)	R^2	R_L	K_f	1/n	R^2
25	178.57	0.0190	0.9836	0.1782	13.266	0.4614	0.9808
35	204.08	0.0351	0.9131	0.0128	24.594	0.3995	0.9529
45	192.31	0.0614	0.9674	0.0679	36.745	0.3321	0.9727

According to the results given in Table 3, although the correlation coefficients (R^2) are high, it is seen that the DR solution studied at 25 °C fits the Freundlich isotherm model more. From this situation, it can be deduced that the adsorption occurs in a multi layer and heterogeneous on the adsorbent surface at 25 °C. The average of the calculated R_L values for all temperatures and all initial dye concentrations is shown in Table 3. Since these average R_L values are between 0 and 1, adsorption takes place spontaneously at every temperature.

Thermodynamic data obtained from DR adsorption are shown in Table 4. Positive values of ΔH° indicated that the process of adsorption is endothermic. A positive ΔS° value indicates the affinity of the dyestuff to the adsorbent. During chemical adsorption at the liquid-solid interface, the disorder increases and the positive ΔS° value is an indicator of this. The ΔG° value decreased with the increase in temperature. This indicates greater driving force at higher temperatures. This impact causes the adsorption capacity to rise as temperature rises.

Table 4. Thermodynamic parameters for the adsorption of DR onto AC

			ΔG (kJ/mol K)		
R^2	ΔH (kJ mol^{-1})	ΔS (kJ mol^{-1} K^{-1})	298 K	308 K	318 K
0.9958	71.332	0.255	-4.624	-7.172	-9.720

4. Conclusion

DR removal from the aqueous solution was investigated by using AC derived from chestnut shell with $ZnCl_2$ activation. For determining optimal adsorption conditions, experiments were performed at different temperature, AC amount, pH, contact time and concentration. Using 0.1 g AC at pH 2.5 and 45°C for an initial concentration of 100 mg/L, 97.4% removal of dye was achieved. Thermodynamic and kinetic constants for the adsorption of DR on AC were analyzed. Kinetic statistics demonstrate that its adsorption occurs in multiple steps. The step limiting the adsorption fits the kinetic model of pseudo-2nd order. The most suitable isotherm was determined as the Freundlich model. Thermodynamic data revealed that the adsorption of DR on AC was endothermic. 45.85 mg/g adsorption capacity was found. In this study, it was shown that AC can be produced from chestnut bark and can be used in DR adsorption. High surface area and microporous AC was found to be a suitable adsorbent for DR adsorption. In our future studies, the usage cycle will be determined by regeneration of the AC.

Decleration of interests

The authors declare that they are not aware of any competing interests.

References

1. **Akbari, P. & Olfati, F. (2020).** Preparing Activated Carbon from Chestnut Shell and Binding Polyacrylic Amidoxime to Its Surface to Remove Some Metals from Aqueous Solution. *Arc. Pharm. Pract.*, 1, 37.
2. **Akkari, I., Graba, Z., Bezzi N., Kaci, M.M., Merzeg, F.A., Bait N., Ferhati, A., Dotto, G.L. & Benguerba, Y. (2023).** Effective Removal of Cationic Dye on Activated Carbon Made from Cactus Fruit Peels: A Combined Experimental and Theoretical Study. *Environ. Sci. Pollut. Res.*, 30 (2), 3027–44.
3. **Al Kausor, M., Gupta S.S., Bhattacharyya, K.G. & Chakrabortty, D. (2022).** Montmorillonite and Modified Montmorillonite as Adsorbents for Removal of Water Soluble Organic Dyes: A Review on Current Status of the Art. *Inorg. Chem. Commun.*, 143, 109686.
4. **Altintig, E., Onaran, M., Sarı, A., Altundag, H. & Tuzen, M. (2018).** Preparation, Characterization and Evaluation of Bio-Based Magnetic Activated Carbon for Effective Adsorption of Malachite Green from Aqueous Solution. *Inorg. Chem. Commun.*, 220, 313–21.
5. **Arab, C., El Kurdi, R. & Patra, D. (2022).** Zinc curcumin oxide nanoparticles for enhanced adsorption of Congo red: kinetics and adsorption isotherms study. *Mater. Today Chem.* 23, 100701.
6. **Aragaw, T.A. & Bogale, F.M. (2021).** Biomass-Based Adsorbents for Removal of Dyes From Wastewater: A Review. *Front. Environ. Sci.*, 9, 764958.
7. **Bal, G. & Thakur, A. (2022).** Distinct Approaches of Removal of Dyes from Wastewater: A Review. *Mater. Today: Proc.*, 50, 1575–79.
8. **Bayantong, A.R.B., Shih Y.J., Dennis C.O., Abarca, R.R.M. Dong, C.D. & Luna, M.D.G. (2021).** Adsorptive Removal of Dye in Wastewater by Metal Ferrite-Enabled Graphene Oxide Nanocomposites. *Chemosphere*, 274, 129518.
9. **Bennani Karim, A., Mounir, B., Hachkar, M., Bakasse, M. & Yaacoubi, A. (2009).** Removal of Basic Red 46 dye from aqueous solution by adsorption onto Moroccan clay. *J. Hazard. Mater.*, 168, 304-309.
10. **Bergaoui, M., Nakhli, A., Benguerba, Y., Khalfaoui, M., Erto, A., Soetaredjo, F.E., Ismadji, S. & Ernst, B. (2018).** Novel Insights into the Adsorption Mechanism of Methylene Blue onto Organo-Bentonite: Adsorption Isotherms Modeling and Molecular Simulation. *J. Mol. Liq.*, 272, 697–707.
11. **Beydaghdari, M., Saboor, F.H., Babapoor, A., Karve, V.V. & Asgari, M. (2022).** Recent Advances in MOF-Based Adsorbents for Dye Removal from the Aquatic Environment. *Energies*, 15 (6), 2023.
12. **Demiral, H., Baykul, E., Gezer, M.D., Erkoç, S., Engin, A. & Baykul, M.C. (2014).** Preparation and Characterization of Activated Carbon from Chestnut Shell and Its Adsorption Characteristics for Lead. *Sep. Sci. Technol.*, 49 (17), 2711–20.
13. **Demiral, H., Demiral, İ., Tümsek, F. & Karabacakoğlu, B. (2008).** Adsorption of Chromium (VI) from Aqueous Solution by Activated Carbon Derived from Olive Bagasse and Applicability of Different Adsorption Models. *Chem. Eng. J.*, 144 (2), 188–96.
14. **Dutta, S., Gupta, B., Srivastava, S.K. & Gupta, A.K. (2021).** Recent Advances on the Removal of Dyes from Wastewater Using Various Adsorbents: A Critical Review. *Mater. Adv.*, 2 (14), 4497–4531.

15. **Errais, E., Duplay, J., Elhabiri, M., Khodja, M., Ocampo, R., Baltenweck-Guyot, R. & Darragi, F. (2012).** Anionic RR120 dye adsorption onto raw clay: Surface properties and adsorption mechanism. *Colloids Surf. A Physicochem.*, 403, 69-78.
16. **Extross, A., Waknis, A., Tagad, C., Gedam, V.V. & Pathak, P.D. (2023)** Adsorption of congo red using carbon from leaves and stem of water hyacinth: equilibrium, kinetics, thermodynamic studies', *Int. J. Environ. Sci. Technol.*, 20 (2) 1607–1644.
17. **Foroutan, R., Peighambardoust, S.J., Peighambardoust, S.H., Pateiro, M. & Lorenzo, J.M. (2021).** Adsorption of Crystal Violet Dye Using Activated Carbon of Lemon Wood and Activated Carbon/Fe3O4 Magnetic Nanocomposite from Aqueous Solutions: A Kinetic, Equilibrium and Thermodynamic Study. *Molecules*, 26 (8), 2241.
18. **Hasani, S., Ardejani F.D. & Olya, M.E. (2017).** Equilibrium and kinetic studies of azo dye (Basic Red 18) adsorption onto montmorillonite: Numerical simulation and laboratory experiments. *Korean J. Chem. Eng.* 34 (8,), 2265–2274.
19. **Hesas, R. H., Arami-Niya, A., Wan Daud, W.M.A. & Sahu, J.N. (2013**). Preparation and Characterization of Activated Carbon from Apple Waste by Microwave-Assisted Phosphoric Acid Activation: Application in Methylene Blue Adsorption. *BioResour.*, 8 (2), 2950–66.
20. **Hidayat, E., Harada, H., Mitoma, Y., Yonemura, S., Halem, H.I.A. (2022).** Rapid Removal of Acid Red 88 by Zeolite/Chitosan Hydrogel in Aqueous Solution. *Polymers*, 14, (5), 893.
21. **Husien, Sh, El-taweel, R.M., Salim, A.I., Fahim, I.S., Said, L.A. & Radwan, A.G. (2022).** Review of Activated Carbon Adsorbent Material for Textile Dyes Removal: Preparation, and Modelling. *Curr. Res. Green Sustain. Chem.*, 5, 100325.
22. **Isik, Z., Saleh, M., M'barek, I., Yabalak, E., Dizge, N. & Deepanraj, B. (2022).** Investigation of the adsorption performance of cationic and anionic dyes using hydrochared waste human hair. *Biomass Conv. Bioref., Mar.*, doi: 10.1007/s13399-022-02582-2.
23. **Jawad, A.H., Abdulhameed, A.S., Wilson, L.D., Syed-Hassan, S.S.A., ALOthman, Z.A. & Khan, M.R. (2021).** High Surface Area and Mesoporous Activated Carbon from KOH-Activated Dragon Fruit Peels for Methylene Blue Dye Adsorption: Optimization and Mechanism Study. *Chin. J. Chem. Eng.*, 32, 281–90.
24. **Kang Y., Zhang, B., Miao, J., Yu, Y., Fu, J., Jia, B. & Li, L. (2023)** Superparamagnetic Fe3O4@Al-Based Metal-Organic Framework Nanocomposites with High-Performance Removal of Azo Dyes. SSRN Journal doi: 10.2139/ssrn.4359337.
25. **Karapınar, H.S., (2022).** Adsorption Performance of Activated Carbon Synthesis by ZnCl2, KOH, H3PO4 with Different Activation Temperatures from Mixed Fruit Seeds. *Environ. Technol.*, 43 (9), 1417–35.
26. **Kavitha, D & Namasivayam, C. (2007).** Experimental and Kinetic Studies on Methylene Blue Adsorption by Coir Pith Carbon. *Bioresour. Technol.*, 98 (1), 14–21.
27. **Kazemipour, M., Ansari, M., Tajrobehkar, S., Majdzadeh, M. & Kermani, H.R. (2008).** Removal of Lead, Cadmium, Zinc, and Copper from Industrial Wastewater by Carbon Developed from Walnut, Hazelnut, Almond, Pistachio Shell, and Apricot Stone. *J. Hazard. Mater.*, 150 (2), 322–27.
28. **Khan, T.A., Nouman, Md., Dua, D., Khan, S.A. & Alharthi, S.S. (2022).** Adsorptive Scavenging of Cationic Dyes from Aquatic Phase by H3PO4 Activated Indian Jujube (Ziziphus Mauritiana) Seeds Based Activated Carbon: Isotherm, Kinetics, and Thermodynamic Study. *J. Saudi Chem. Soc.*, 26 (2), 101417.
29. **Kong, L. & Zhang, M. (2022).** Adsorption of Methylene Blue on Chestnut Shell-Based Activated Carbon: Calculation of Thermodynamic Parameters for Solid–Liquid Interface Adsorption. *Catalysts*, 12 (8), 813.
30. **Lafi, R., Montasser, I. & Hafiane, A. (2019).** Adsorption of Congo Red Dye from Aqueous Solutions by Prepared Activated Carbon with Oxygen-Containing Functional Groups and Its Regeneration. *Adsorp. Sci. Technol.*, 37 (1–2), 160–81.
31. **Li, C.J., Zhang, Y.J., Chen, H., He, P.Y. & Meng, Q. (2022).** Development of Porous and Reusable Geopolymer Adsorbents for Dye Wastewater Treatment. Journal of Cleaner Production 348, 131278.
32. **Lian, L., Guo, L., Guo, C. (2009).** Adsorption of Congo red from aqueous solution onnto Ca-bentonite. *J.Hazard. Mater.*, 161, 126-131.
33. **Liu, T., Li, Y., Du,Q., Sun, J., Jiao, Y., Yang, G., Wang, Z., Xia, Y., Zhang W., Wang K., Zhu H. & Wu D. (2012).** Adsorption of Methylene Blue from Aqueous Solution by Graphene. *Colloids Surf. B.*, 90, 197–203.
34. **Lu, F., Dong, A., Ding, G., Xu, K., Li, J. & You, L. (2019).** Magnetic porous polymer composite for high performance adsorption of acid red 18 based on melamine resin and chitosan. *J. Mol. Liq.*, 294, 111515.
35. **Maximova, A. & Koumanova, B. (2008).** Equilibrium and kinetics study of adsorption of basic dyes onto perfil from aqueous solutions. *J. Univ. Chem. Technol. Metall.*, 43 (1). 101–108.
36. **Özçimen, D. & Meriçboyu, A.E. (2009).** Removal of Copper from Aqueous Solutions by Adsorption onto Chestnut Shell and Grapeseed Activated Carbons. *J. Hazard. Mater.*, 168 (2–3), 1118–25.

37. **Prahas, D., Kartika, Y., Indraswati, N. & Ismadji, S. (2008**). Activated Carbon from Jackfruit Peel Waste by H_3PO_4 Chemical Activation: Pore Structure and Surface Chemistry Characterization. *Chem. Eng. J.*, 140 (1–3), 32–42.
38. **Rivera, M., Pazos, M. & Sanromán, M.A., (2011).** Development of an Electrochemical Cell for the Removal of Reactive Black 5. *Desalination*, 274 (1–3), 39–43.
39. **Saini, B., Dey, A. (2022).** Synthesis and Characterization of Copolymer Adsorbent for Crystal Violet Dye Removal from Water. Materials Today: Proceedings 61, 342–50.
40. **Saratale, R.G., Sivapathan, S.S., Jung, W.J., Kim, H.Y., Saratale, G.D. & Kim, D.S. (2016).** Preparation of activated carbons from peach stone by $H_4P_2O_7$ activation and its application for the removal of Acid Red 18 and dye containing wastewater. *J. Environ. Sci. Health A.*, 51 (2), 164–177.
41. **Selengil, U. & Yıldız, D. (2022).** Investigation of the Methylene Blue Adsorption onto Waste Perlite. *Desalin. Water Treat.*, 262, 235–47.
42. **Şencan, A., Karaboyacı, M. & Kılıç, M. (2015).** Determination of Lead (II) Sorption Capacity of Hazelnut Shell and Activated Carbon Obtained from Hazelnut Shell Activated with $ZnCl_2$. *Environ. Sci. Pollut. Res.*, 22 (5), 3238–48.
43. **Sh. Gohr, M., Abd-Elhamid, A.I., El-Shanshory, A.A., & Soliman, H.M.A. (2022).** Adsorption of Cationic Dyes onto Chemically Modified Activated Carbon: Kinetics and Thermodynamic Study. *J. Mol. Liq.*, 346, 118227.
44. **Shafeeyan, M. S., Daud, W.M.A.W., Houshmand, A. & Arami-Niya, A. (2011).** Ammonia Modification of Activated Carbon to Enhance Carbon Dioxide Adsorption: Effect of Pre-Oxidation. *App. Surf. Sci.*, 257 (9), 3936–42.
45. **Shakoor, Sadia, & Abu Nasar. (2016).** Removal of Methylene Blue Dye from Artificially Contaminated Water Using Citrus Limetta Peel Waste as a Very Low Cost Adsorbent. *J. Taiwan Inst. Chem.*, 66, 154–63.
46. **Sharma, A. & Bhattacharyya, K.G. (2005).** Adsorption of Chromium (VI) on Azadirachta Indica (Neem) Leaf Powder. Adsorption 10 (4), 327–38.
47. **Sun, Y., Li, H., Li, G., Gao, B., Yue, Q. & Li, X. (2016).** Characterization and Ciprofloxacin Adsorption Properties of Activated Carbons Prepared from Biomass Wastes by H_3PO_4 Activation. *Biores. Technol.*, 217, 239–44.
48. **Tumsek, F. (2019).** Investigation of deep red adsorption using bentonite clay modified with a surfactant. *Fresenius Environ. Bull.*, 28 (11), 7816-7822.
49. **Xue, H., Gao, X., Seliem, M.K., Mobarak, M., Dong, R., Wang, X., Fu, K., Li, Q. & Li, Z. (2023).** Efficient Adsorption of Anionic Azo Dyes on Porous Heterostructured MXene/Biomass Activated Carbon Composites: Experiments, Characterization, and Theoretical Analysis via Advanced Statistical Physics Models. *Chem. Eng. J.*, 451, 138735.
50. **Yorgun, S., Karakehya, N. & Yıldız, D. (2017).** Adsorption of Methylene Blue onto Activated Carbon Obtained from $ZnCl_2$. *Desalin. Water Treat.*, 58, 274–84.
51. **Yuh-Shan, H. (2004).** Citation Review of Lagergren Kinetic Rate Equation on Adsorption Reactions. *Scientometrics*, 59 (1), 171–77.
52. **Zhang, M., Liu, X., Li, B., Li, W. Tan, Z., Wang, Q., Zhang, L. (2021**). Removal of Toxic Dyes from Aqueous Solutions by Adsorption onto a Novel Activated Carbon Prepared from Chestnut Shell. *Desalin. Water Treat.*, 222, 246–58.